Coupled Steam and Oxidative Reforming for Hydrogen Production in a Novel Membrane Circulating Fluidized-Bed Reformer

Pradeep Prasad* and Said S. E. H. Elnashaie

Chemical Engineering Department, Auburn University, 230 Ross Hall, Auburn, Alabama 36849

A novel circulating fluidized-bed membrane reactor employing a reactor−regenerator type of configuration is proposed for hydrogen production by the steam reforming of natural gas. The removal of hydrogen through hydrogen-permeable membranes pushes the equilibrium toward higher production of hydrogen. In the present paper, modeling studies are carried out on the reactor section of this configuration. Cases with and without hydrogen-selective membranes (cocurrent and countercurrent) are considered and compared. The model results show the great advantages associated with the breaking of the thermodynamic limitations coupled to the hydrodynamic limitations associated with the previous generations of bubbling fluidized-bed reformers. It is shown that autothermal operation can be achieved through simultaneous oxidative reforming, giving high hydrogen yields and productivities with low net consumption of energy.

Introduction

The classical industrial process for steam reforming (fixed bed) consists of hundreds of parallel catalyst tubes surrounded by a very large top- or side-fired furnace supplying the necessary endothermic heat. The reaction is carried out at temperatures in the range of 800−1000 K and at pressures in the range of 20−25 bar. Relatively large Ni-based catalyst particles are used to avoid an excessive pressure drop along the reformer tubes. This design, which is the dominant configuration in industry at present, suffers from a number of limitations that lead to the lack of efficiency and huge size of the equipment. Because of the large size of the catalyst pellets, intraparticle diffusion limitations reduce the apparent catalyst activity, and hence effectiveness factors,[1] to values as low as 10^{-2}−10^{-3}. The reversible nature of the reactions limits the conversion to that of the thermodynamic equilibrium and necessitates the use of elevated temperatures to achieve acceptable levels of conversion. Also, carbon formation increases with an increase in the temperature, leading to deactivation of the catalyst and thus necessitating the use of a high steam-to-hydrocarbon ratio. This tendency increases for hydrocarbons higher than methane.

Elnashaie and Adris[2] were the first to propose the use of a bubbling fluidized-bed steam reformer using a powdered catalyst, to overcome the diffusional limitations of the catalyst pellets and thus increase the effectiveness factor 100−1000-fold. This second-generation reformer underwent further remarkable enhancements in performance, by the use of composite hydrogen permselective membranes to "break" the thermodynamic equilibrium barrier and push the reaction toward higher conversions, even at lower temperatures.[3] Adris[4] and Adris et al.[5] further studied, validated, and patented[6] the fluidized-bed membrane reformer (FBMR) after building a pilot plant and undertaking experimental and modeling studies of the system. Roy et al.[7] have experimentally studied the addition of oxygen to the FBMR to provide the heat required for the endothermic reactions and found that autothermal conditions could be reached and maintained. The FBMR configuration, although very efficient, still suffers from limitations with regard to the flow rate that can be used in a bubbling fluidized bed, thereby preventing full exploitation of the increase in the catalyst effectiveness factor. Furthermore, it is not suitable for higher hydrocarbons because it does not have the best provision for handling the excessive carbon formation associated with higher hydrocarbons. Our present and future work will suggest several improvements in this second-generation configuration and introduce the third-generation reformer, which is much more efficient, productive, and flexible than the previous two generations.

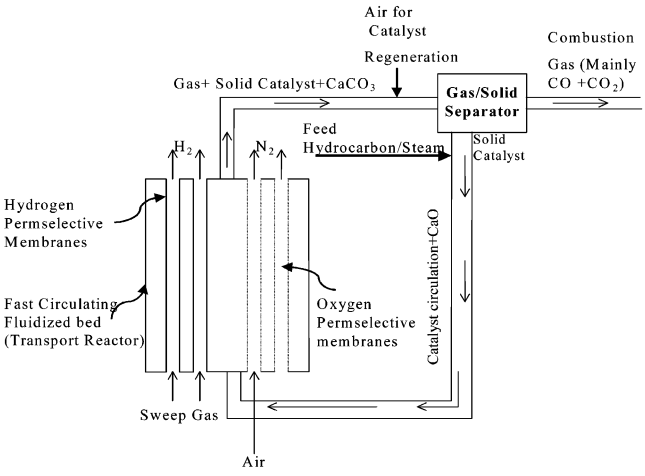

Figure 1. Schematic diagram of the proposed novel configuration.

Main Features of the Present Novel Configuration (Third-Generation Reformer)

The proposed novel configuration (see Figure 1) is a circulating fluidized bed (CFB) using powdered catalyst particles to overcome both the diffusion and hydrody-

* To whom correspondence should be addressed. Tel.: 1-334-8442051. Fax: 1-334-8442063. E-mail: ppradeep@eng.auburn.edu.

10.1021/ie030071h CCC: $25.00
Published on Web 08/27/2003

namic limitations. The thermodynamic equilibrium limitations of the reforming reactions are broken using hydrogen permselective membranes[8−14] and/or a CO_2 acceptor such as CaO.[15,16] In addition, oxidative reforming and complete oxidation of part of the methane feed is carried out in situ in order to supply heat for the reforming reactions.[17−22] Oxygen is supplied through oxygen permselective membranes[23,24] along the length of the reformer. Not only is the supply of oxygen through the permselective membranes desirable from a safety point of view, but it could also allow optimization of the system in such a way that the extent of the partial oxidation reaction is optimized and the loss of methane feed through complete oxidation is minimized. In addition, the use of oxygen permselective membrane tubes allows the use of air instead of pure oxygen and the possibility of producing pure nitrogen as an additional byproduct. The problem of catalyst deactivation by coke deposition[25,26] can be addressed by separating the catalyst from the gas stream and regenerating it by burning of the carbon as the catalyst is on its way back to the reforming section. The present novel design is quite versatile in terms of the feedstocks that may be used as a result of this provision for handling excessive carbon formation. A more detailed description of the configuration is given elsewhere.[27−30]

The Model

The present paper considers the riser reformer with steam and oxidative reforming of methane and cocurrent/countercurrent hydrogen permselective membranes. Different parameters for measuring the efficiency of the reformer are employed. The model utilizes a kinetic approach in contrast to the equilibrium-based approach that has been used by Grace et al.[31] which uses free-energy minimization techniques to predict the chemical equilibrium and also the effect of the removal of hydrogen. The use of a kinetic-based approach allows us to include some phenomena like the effect of temperature on membrane permeation. Both steam reforming and oxidative reforming kinetics are included in the formulation of the model equations.

Methane Steam Reforming. The nonmonotonic rate expressions proposed by Xu and Froment[32] for the Ni/Al_2O_3 catalyst and analyzed in some detail by Elnashaie et al.[33] are used in the present study. The three main reactions are given below. The corresponding rate equations and kinetic parameters are available in the work by Xu and Froment.[32] The net reaction is highly endothermic as shown in eqs 1−3.

$$CH_4 + H_2O \rightleftharpoons CO + 3H_2 \quad (\Delta H^0 = 206 \text{ kJ/mol}) \quad (1)$$

$$CO + H_2O \rightleftharpoons CO_2 + H_2 \quad (\Delta H^0 = -41 \text{ kJ/mol}) \quad (2)$$

$$CH_4 + 2H_2O \rightleftharpoons CO_2 + 4H_2 \quad (\Delta H^0 = 165 \text{ kJ/mol}) \quad (3)$$

Partial Oxidation. A number of supported metal catalysts such as Ni, Rh, Pt, etc., have been reported for partial oxidation of methane.[17] Dissanayake et al.[20] examined the oxidation state and phase composition of the Ni/Al_2O_3 catalyst as a function of axial position in the catalyst bed. Their results support the mechanism of methane combustion followed by steam and carbon dioxide reforming. The following reaction rates and the relevant constants from Jin et al.[23] have been used in addition to the steam reforming rates.

Partial oxidation:

$$CH_4 + 0.5O_2 \rightarrow CO + 2H_2 \quad (\Delta H^0 = -36 \text{ kJ/mol}) \quad (4)$$

Combustion:

$$CH_4 + 2O_2 \rightarrow CO_2 + 2H_2O \quad (\Delta H^0 = -802 \text{ kJ/mol}) \quad (5)$$

$$r_5 = A_5 p_{CH_4} p_{O_2} \exp(-E_5/RT) \quad (6)$$

Dry reforming of methane:

$$CH_4 + CO_2 \rightleftharpoons 2CO + 2H_2 \quad (\Delta H^0 = 247 \text{ kJ/mol}) \quad (7)$$

$$r_7 = A_7 p_{CH_4} p_{CO_2} \exp(-E_7/RT)\left(1 - \frac{p_{CO}^2 p_{H_2}^2}{K_7 p_{CH_4} p_{CO_2}}\right) \quad (8)$$

Assumptions. The following simplifying assumptions are included in the model derivation:

(i) All parts of the system are at steady state.

(ii) The reformer gas and catalyst are flowing in plug flow through the reformer.

(iii) There is negligible axial mixing and complete radial mixing.

(iv) The volume fraction of the solid (catalyst) remains constant along the length of the reactor ($\epsilon = 0.8$).

(v) The membranes are completely permselective and are in thermal equilibrium with the reformer gases.

(vi) Heat losses are negligible.

(vii) Ideal gas laws are applicable.

Model Equations. Mass balance involves six components, viz., CH_4, H_2O, CO, CO_2, H_2, and O_2. Thus, there are six mass balance equations for the reactor side and one each for the two membrane sides apart from the energy balance equation. The partial pressures involved are calculated using the ideal gas relation.

$$\frac{dF_i}{dl} = \rho_c A_c (1 - \epsilon) R_i - m J_i \quad (9)$$

$$\sum_i F_i \frac{d(H_i)}{dl} = A_c \rho_c (1 - \epsilon) \sum_j r_j (-\Delta H_j) \quad (10)$$

In eq 9, $J_i = 0$ for all components in the reactor side equations except hydrogen and oxygen for which J_i is the corresponding molar permeation term depending on the type of membrane used. Also, $R_i = 0$ in the mass balance equations for hydrogen and oxygen in their respective membrane side equations. The value of m is -1 in the membrane side equation for the cocurrent case and $+1$ otherwise. For a supported dense Pd membrane, the hydrogen permeation term is given below.[14] The values of the parameters were extracted from work by Nam and Lee[11] for use in the present study.

$$J_{H_2} = Q_{H_2}\left(\frac{\pi d_m n_{t,H_2}}{\delta_{H_2}}\right) \exp\left(\frac{-E_{H_2}}{RT}\right)(p^n_{H_2,r} - p^n_{H_2,m}) \quad (11)$$

For a dense Perovskite oxygen-permeable membrane, the oxygen permeation term when diffusion through the membrane is limiting is given by Tsai et al.[24] as

Table 1. Constants Used for the Membranes

	Q_0	E (kJ·mol^{-1})	d (μm)	n
hydrogen-permeable membrane[11]	2.06×10^{-5} kmol·m^{-1}·kPa^{-n}·h^{-1}	22.84	2.0	1.0
oxygen-permeable membrane[24]	2.6424×10^{-6} kmol·m^{-1}·K^{-1}·h^{-1}	62.7	50[a]	

[a] Assumed.

$$J_{O_2} = Q_{O_2}(\pi d_m n_{t,O_2}) \exp\left(\frac{-E_{O_2}}{RT}\right)\frac{T}{\delta_{O_2}} \ln\left(\frac{P_{O_2,m}}{P_{O_2,r}}\right) \quad (12)$$

The set of differential equations is solved using the feed conditions per tube of an industrial fixed-bed reformer described by Elnashaie and Elshishini.[1] The following data are used unless otherwise stated: the cross-sectional area (A_c) of the reactor available for flow of reactants is 75.12 cm^2, the reactor pressure (P) is 10 atm, the diameter of the hydrogen membrane tubes (d_m) is 5 mm, the number of hydrogen-permeable tubes is 80, the pressure on the hydrogen-permeable membrane side is 1 atm, and the flow rate of the inert sweep gas is 1 kmol/h. On the oxygen-permeable membrane side, the diameter of the membrane tubes (d_m) is 5 mm, the number of tubes is 80, the pressure is 30 atm, and the flow rate of air is 10 kmol/h. To effectively explore the effect of the oxygen-permeable membranes, a thickness of 50 μm is considered, assuming that a membrane with the same parameters but a smaller thickness than that reported by Tsai et al.[24] can be fabricated. Such a thin membrane would need to be supported[34,35] on a porous support, which itself has negligible resistance. The data used for the two hydrogen- and oxygen-permeable membranes are summarized in Table 1. A cocurrent mode of operation is assumed for the membranes unless explicitly stated otherwise. The total hydrogen yield is calculated as the total amount of hydrogen produced per mole of methane introduced.

$$Y_{H_2} = \frac{F_{H_2,m} + F_{H_2,r} - F^0_{H_2}}{F^0_{CH_4}} \quad (13)$$

The maximum area occupied by the membranes as a percentage of the total cross-sectional area is about 30%, leaving the remaining 70% available for gas−solid flow. The generalized map of gas−solid contacting reported by Kunii and Levenspiel[36] is used to ensure that the reactor is in either the fast fluidization or the pneumatic transport regime.

Solution of the Model Equations. For the cocurrent case, the set of nonlinear initial value differential equations is integrated using the IVPAG subroutine from the IMSL libraries. The countercurrent case involves more computational effort as the problem is described by a two-point boundary value problem because the membrane sweep gas feed with a zero hydrogen concentration condition is defined at the exit of the reformer. An efficient iterative technique has been used to solve this system by assuming a starting guess for the hydrogen molar flow rate at the feed end of the reformer, integrating forward along the length of the reformer, and iterating to converge toward the solution. However, it was noted that, for this countercurrent case, several "false" solutions are numerically possible. This is seen in Figure 2, where a number of assumed membrane-side outlet conditions for hydrogen satisfy the criterion of zero hydrogen in the feed sweep gas, though the actual solution is only the point where the curve first meets the x axis (point a) within some level of numerical tolerance.

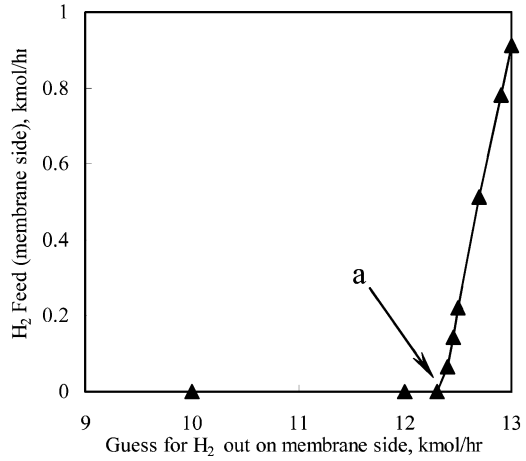

Figure 2. Countercurrent case: possibility of false solutions.

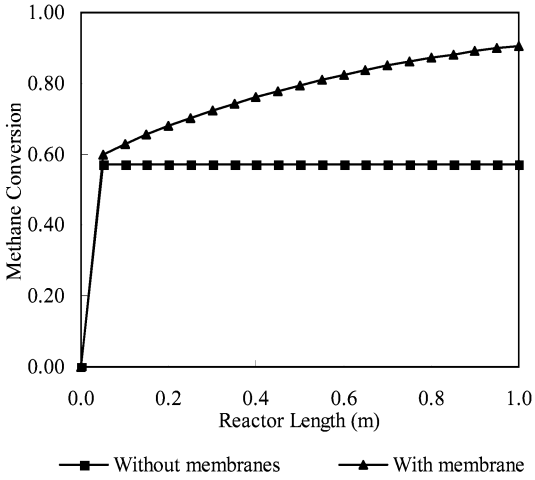

Figure 3. Isothermal reactor (T = 900 K, P = 5 atm, and n_t = 20): effect of the hydrogen-permeable (Pd) membrane.

Results and Discussion

Isothermal Cocurrent and Countercurrent Cases. The isothermal case is an artificial case where heat is assumed to be supplied in such a way as to keep the temperature constant along the length of the reactor. Figure 3 shows that in the absence of hydrogen-permeable membranes the methane conversion reaches its equilibrium value in an extremely short distance. This is to be expected because the reaction rate increases 100−1000-fold because of the increase in the effectiveness factor. It is shown in Figure 3 that an improvement in methane conversion (over 90% at the exit) can be achieved by the use of hydrogen-permeable membranes.

Countercurrent flow on the membrane side involves the solution of a two-point boundary value problem as explained earlier. The countercurrent mode of operation has the advantage of a better hydrogen partial pressure driving force as compared to the cocurrent mode. In

Table 2. Comparison between the Cocurrent and Countercurrent Modes of Operation with Respect to Hydrogen-Permeable Membranes and in the Absence of Oxygen-Permeable Membranes[a]

case	X_{CH_4}(eq)	mode	X_{CH_4}	Y_{H_2}	$F_{H_2\ membrane}$ (kmol·h^{-1})	% of H_2 permeated	% increase in X_{CH_4}	% increase in Y_{H_2}	% increase in $F_{H_2\ membrane}$
1	0.424	cocurrent	0.824	3.184	10.207	75.34	6.92	7.52	15.41
		countercurrent	0.881	3.424	11.780	81.27			
2	0.505	cocurrent	0.988	3.841	14.416	89.29	1.11	3.42	13.28
		countercurrent	0.999	3.973	16.330	97.99			

[a] Case 1: $P = 5$ atm, $T = 850$ K, $n_t = 40$. Case 2: $P = 7$ atm, $T = 900$ K, $n_t = 40$.

Table 2, for case 1 the methane conversion, hydrogen yield, and membrane-side hydrogen flow rate (permeated hydrogen) for the countercurrent case increase over those of the cocurrent case by 6.92%, 7.52%, and 14.41%, respectively. Case 2 corresponds to a case where the cocurrent configuration itself shows almost complete conversion. In such a case, the use of countercurrent membrane operation will not have much effect on the methane conversion and hydrogen yield but still has a strong effect on the H_2 permeation, which is reflected in the increase in the percentage of hydrogen permeated. This situation is also important because it is desirable to have as much pure hydrogen as possible in the membrane side.

Adiabatic Operation Using an Oxygen Supply. The oxidation reactions (4) and (5) provide an in situ supply of heat for the reaction. There are two ways to add the oxygen. One is to supply pure oxygen along with the feed, as was done by Roy et al.,[7] Bharadwaj and Schmidt,[18] and Mleczko and Wurzel,[22] and the other is to supply it through oxygen-permeable membrane tubes.[23,24,34] When oxygen-permeable membranes are used, it would be more economical to use air directly as a source of oxygen. An important point to be noted is that when we supply heat for the reaction through oxidation instead of the traditional way of supplying heat externally, we are actually using up some of the feed methane for producing heat via oxidation. However, we save on the enormous amount of fuel that needs to be burned in the furnace for providing the endothermic heat in a traditional reformer. In the subsequent results of this paper, adiabatic operation of the reformer is investigated with the heat supply solely from the in situ oxidation of a part of the methane feed.

Figure 4 shows that when no oxygen is fed, the temperature profile shows an abrupt drop near the entrance of the reformer. In the presence of the hydrogen-permeable (Pd) membrane, the temperature drop is even more because of the higher extent of reaction. However, when oxygen is introduced in the feed, a part of the methane undergoes oxidation and releases heat. Consequently, the temperature can increase near the feed side of the reformer. After the initial increase, the temperature remains constant for the case without the hydrogen-permeable membranes as the system reaches equilibrium. The temperature decreases for the case with hydrogen-permeable membranes as a result of the effect of breaking the thermodynamic equilibrium barrier.

The case with oxygen input shows a higher hydrogen yield than the one without oxygen input as a result of the higher temperature. The yield of hydrogen shows a maximum at an oxygen-to-methane molar ratio of about 0.45 (see Figure 5). The maximum in the yield of hydrogen corresponds to almost complete conversion of methane. So, any methane fed beyond the ratio of about

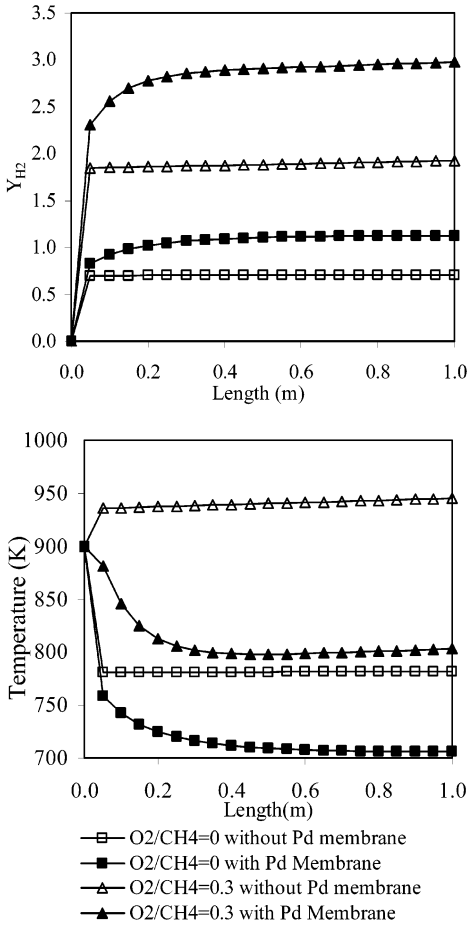

Figure 4. Adiabatic reactor ($T_f = 900$ K): effect of oxygen in the feed.

0.45 oxygen to methane (in the presence of H_2-permeable (Pd) membranes) will only result in greater oxidation of methane, causing a greater loss of the methane feed than what is necessary, which only serves to increase the temperature while having a negative effect on the hydrogen yield. In the case where there are no hydrogen-permeable membranes, not only is the maximum hydrogen yield lower but it also occurs at a different ratio. This is because, in the absence of the hydrogen-permeable membranes, a higher temperature and hence a greater sacrifice of the feed methane to oxidation are required. In this case also, the maximum hydrogen yield corresponds to nearly complete conversion of methane.

Figure 6 shows the effect of introducing oxygen partly through membranes and partly with the feed. Again, we see a maximum in the hydrogen yield with respect to the oxygen-to-methane feed ratio. The hydrogen yield for the case with oxygen-permeable membranes is higher than the corresponding case without the oxygen-permeable membrane until we reach the maximum for the case with oxygen-permeable membranes (e.g., for

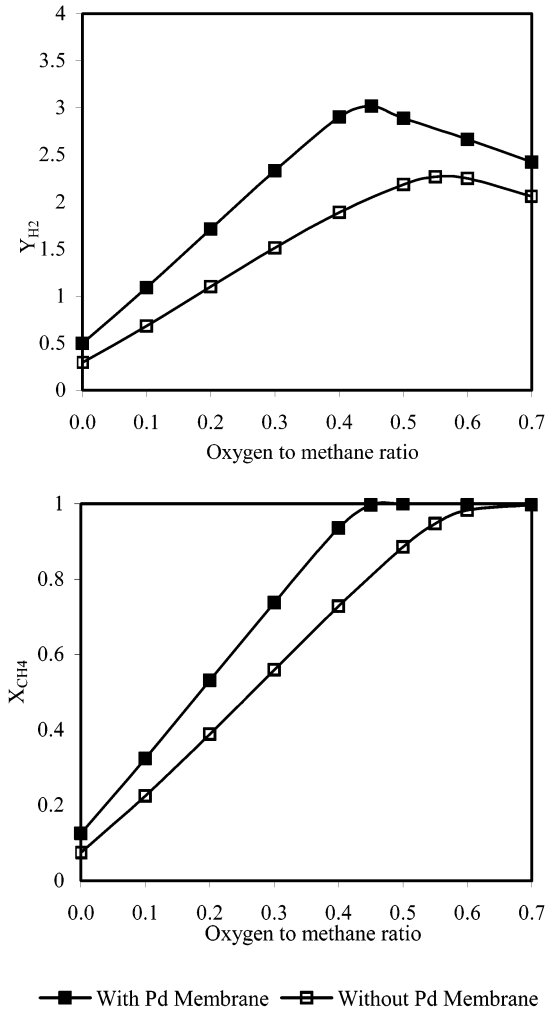

Figure 5. Adiabatic reactor (T_f = 760 K): effect of the oxygen-to-methane ratio in the feed.

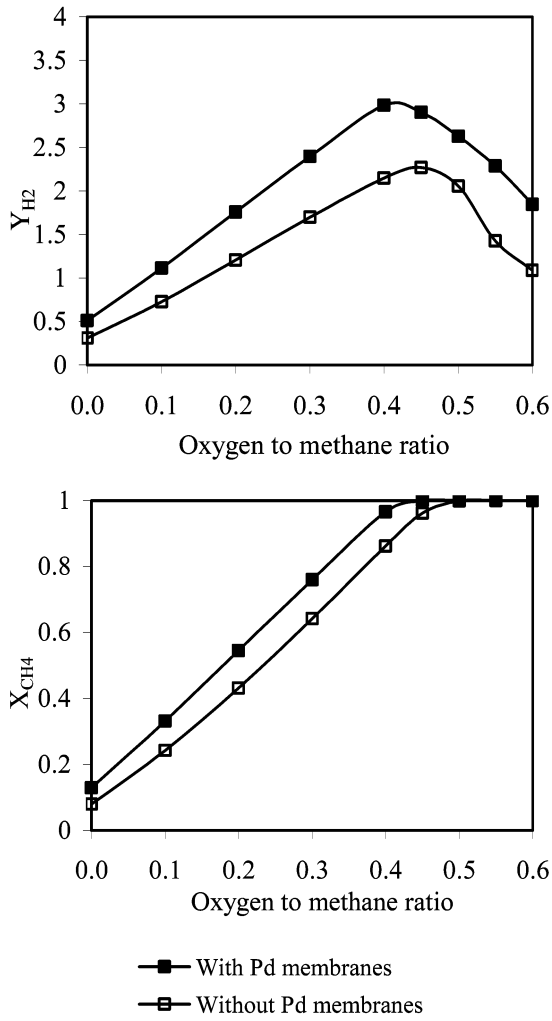

Figure 6. Adiabatic reactor (T_f = 760 K): effect of the oxygen-to-methane ratio in the feed (in the presence of oxygen-permeable membranes).

the case without the hydrogen-permeable (Pd) membranes, the hydrogen yield at a 0.45 oxygen-to-methane ratio is 2.27 in the presence of oxygen-permeable membranes as compared to 2.05 without oxygen-permeable membranes). This difference in yield is due to the additional oxygen that is supplied through the membranes. At low temperatures the oxygen flux is very small for the scale of operations considered here, but as the oxygen in the feed is increased, the temperature increases and the oxygen flux through the membranes also increases, causing greater oxidation of the methane. Thus, at higher oxygen-to-methane feed ratios, the use of the membrane has a negative effect on the hydrogen yield.

In Figure 7 the hydrogen yield per mole of methane converted is plotted (instead of the hydrogen yield per mole of methane fed as in Figures 4−6). Figure 7 compares the cases with and without oxygen-permeable membranes for different reformer oxygen feed ratios and in the presence of the hydrogen-permeable membranes. At low oxygen feed ratios, the hydrogen yield per mole of methane converted is close to 4, which is the theoretical maximum for the reforming reaction. This indicates that reforming is the main process occurring at low oxygen feed ratios. As the oxygen in the feed is raised, more and more methane is consumed by the oxidation reactions, leading to a decrease in hydrogen yield per mole of methane converted, accompanied by an increase in temperature. After complete conversion of methane

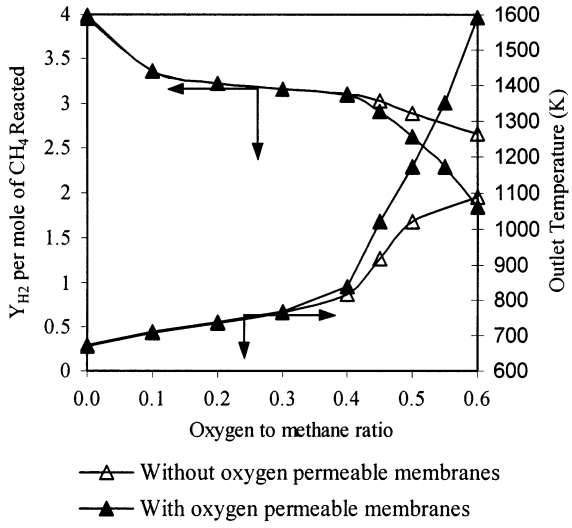

Figure 7. Adiabatic reactor (T_f = 760 K): effect of the oxygen-to-methane ratio in the feed on hydrogen yield per mole of methane reacted.

is attained, the rate of temperature rise increases especially in the case with oxygen-permeable membranes, where an increase in temperature increases the oxygen flux, which again serves to increase the temperature.

A comparison between an adiabatic fast fluidized membrane steam reformer (FFMSR) is performed against both the industrial fixed-bed reactor data and the bubbling fluidized-bed membrane steam reformer (BFBMSR) pilot-plant data (see Table 3). For the FFMSR, the hydrogen-permeable membranes are in countercurrent mode whereas the oxygen-permeable membranes are in cocurrent mode. The oxygen was introduced partly through the oxygen-permeable tubes and partly through the feed.

A few additional important hydrogen production parameters, namely, EH, NHP_1, and NHP_2, are utilized for meaningful comparison between different reformers. EH is the hydrogen equivalent of the net energy (kJ) consumed based on the standard heat of combustion of hydrogen. It provides a picture of the energy penalty associated with production of hydrogen. In the case of the fixed bed, the total energy requirement for a single reactor tube is calculated using the standard heat of combustion of the furnace fuel (assuming that the preheating of the feed and steam generation is achievable through effective heat integration of the furnace off-gases). Because operation is adiabatic for FFMSR and BFBMSR, the only heat requirement is for the preheating of the feed (including oxygen) and generation of steam. EH can thus be calculated as the net energy consumed divided by the standard heat of combustion of hydrogen.

$$\mathrm{EH} = \frac{\text{net energy consumption (kJ/h)}}{\Delta H^{c}_{H_2}\ \text{(kJ/kmol)}} \qquad (14)$$

NHP_1 is the net hydrogen production per mole of methane fed. It is the difference between the total hydrogen production from the process and the hydrogen equivalent of the energy consumed per kilomole of methane fed. NHP_2 is defined as the net hydrogen production (NHP_1) per unit volume of the reformer. Because NHP_1 and NHP_2 are normalized with respect to the methane feed flow rate, they allow a comparison of the hydrogen production efficiency between reformers with different scales of operation.

$$\mathrm{NHP}_1 = \frac{H_2\ \text{produced} - \mathrm{EH\ (kmol/h)}}{CH_4\ \text{feed flow rate (kmol/h)}} \qquad (15)$$

$$\mathrm{NHP}_2 = \frac{\mathrm{NHP}_1}{\text{volume (m}^3\text{)}} \qquad (16)$$

Case A in Table 3 is a comparison between FFMSR and an industrial fixed-bed reformer described by Elnashaie and Elshishini.[1] Even though the methane molar feed flow rate and the cross-sectional area are the same for both of the reformer tubes, the difference in the size of the catalyst particle makes FFMSR operate in the fast fluidization regime. The comparison shows the effect of not only overcoming the diffusion resistance of the catalyst pellets in the fixed bed but also breaking of the thermodynamic equilibrium barrier by use of the hydrogen permselective membranes and the in situ supply of heat through oxidative reforming. The oxygen-to-methane reformer feed ratio in FFMSR is 0.4, and the numbers of hydrogen- and oxygen-permeable tubes are 20 and 140, respectively. A key performance parameter to note is the hydrogen yield per cubic meter of the reactor, which is an important indication of the efficiency of the reactor. The negative value of NHP_1 for the fixed bed indicates that generation of hydrogen involves a net expenditure of energy. For FFMSR, the NHP_1 value is positive. Furthermore, this is achieved in a smaller reformer volume, as shown by the NHP_2 values.

Table 3. Comparison between the Three Reactor Configurations

	case A		case B	
	fixed bed[1]	FFMSR	BFBMSR[7]	FFMSR
methane conversion	0.853	1.00	0.653	0.982
total hydrogen yield	2.812	3.154	1.6	2.863
methane feed rate ($mol \cdot h^{-1}$)	3953	3953	40	3953
oxygen-to-methane feed ratio		0.4	0.45	0.4
process gas exit temperature (K)	1130	892.5	923	908
pressure (kPa)	2200	2200	500	500
length (m)	13.72	1.0	1.14	1.0
reactor volume (m^3)	0.1031	0.0107	0.0139	0.0107
hydrogen yield per cubic meter of reactor	27.3	294.8	109	267.6
EH ($kmol \cdot h^{-1}$)	17.67	5.11	0.046	5.206
NHP_1 (net kmol of H_2 produced/ kmol of CH_4 fed)	−1.67	1.85	0.45	1.54
NHP_2 (NHP_1/m^3)	−16.16	172.54	32.37	143.48

Case B in Table 3 is a comparison between the FFMSR model results and the BFBMSR data from a pilot-plant study.[7] As in case A, the oxygen-to-methane reformer feed ratio was 0.4, and the numbers of hydrogen- and oxygen-permeable tubes were 20 and 140, respectively. An advantage of FFMSR is that higher feed flow rates can be used when operating in the fast fluidization regime, leading to higher production rates. Since the BFBMSR was a pilot plant with a relatively small CH_4 feed and H_2 production capacity, the energy consumption (EH) in Table 3 is lower for the BFBMSR than the FFMSR. The total hydrogen yield per cubic meter and the NHP_1 and NHP_2 values of the reactor take care of the difference in the scales of operation according to their definitions and hence allow the comparison of the efficiencies of the reactor for hydrogen production. It is clear that FFMSR is much more efficient than BFBMSR. The progression from one generation of reformers to the next is quite clear through the table, and the two cases of comparison clearly show the potential superiority of the suggested novel FFMSR configuration.

Conclusion

Modeling studies were carried out on a proposed novel FFMSR to show that autothermal operation can be attained by the introduction of oxygen as part of the feed and through oxygen-permeable membranes. The introduction of oxygen through oxygen-permeable membranes was limited by the low flux of the membranes especially at lower temperatures. The countercurrent mode of operation with respect to the hydrogen-permeable Pd membranes was also studied and was shown to be more efficient than the cocurrent operation. A comparison was made of the simulation results for an adiabatic FFMSR and the industrial results for a fixed bed and the pilot plant results for a bubbling fluidized-bed reformer using a number of hydrogen production and energy consumption parameters. The comparison shows that the proposed FFMSR configuration is very

promising from hydrogen production and energy consumption points of view.

Acknowledgment

This research was supported by Auburn University through Grant 2-12085.

Nomenclature

A_c = area of a cross section of the reactor (m^2)
A_j = preexponential factor in the rate constant for reaction j
d_m = diameter of the membrane tube (m)
E = activation energy ($kJ \cdot mol^{-1}$)
EH = net energy consumed in terms of equivalent kilomoles of hydrogen ($kmol \cdot h^{-1}$)
$F_{H_2,r}$, $F_{H_2,m}$ = molar flow rate of hydrogen on the reactor and membrane sides ($kmol \cdot h^{-1}$)
F_i, F_i^0 = molar flow rate and molar feed flow rate of species i ($kmol \cdot h^{-1}$)
$\Delta H^c_{H_2}$ = standard heat of combustion of hydrogen (=285.84 $kJ \cdot mol^{-1}$)
ΔH_j = heat of reaction for reaction j ($kJ \cdot mol^{-1}$)
l = distance along the reactor (m)
NHP_1 = net hydrogen production per mole of methane fed
NHP_2 = net hydrogen production per unit volume of the reformer (m^{-3})
$p_{H_2,r}$, $p_{H_2,m}$ = hydrogen partial pressure on the reactor and membrane sides, respectively (kPa)
p_i = partial pressure of species i (kPa)
Q_{H_2}, Q_{O_2} = preexponential factors in the Arrhenius relationship for the membranes
J_i = flux of component i through the membrane ($kmol \cdot h^{-1} \cdot m^{-2}$)
r_j = rate of reaction j ($kmol \cdot h^{-1} \cdot kg_{cat}^{-1}$)
R = gas constant ($kJ \cdot kmol^{-1} \cdot K^{-1}$)
R_i = rate of production of species i ($kmol \cdot h^{-1} \cdot kg_{cat}^{-1}$)
T = temperature (K)
T_f = feed temperature (K)
X_{CH_4}, X_{H_2O} = conversion of methane and steam
Y_{H_2} = yield of hydrogen
δ_{H2}, δ_{O_2} = thicknesses of the membranes (m)
ϵ = void fraction
ρ_c = density of the catalyst ($kg \cdot m^{-3}$)

Literature Cited

(1) Elnashaie, S. S. E. H.; Elshishini, S. S. *Modelling, Simulation and Optimization of Industrial Fixed Bed Catalytic Reactors*; Gordon and Breach Science Publishers: London, 1993.

(2) Elnashaie, S. S. E. H.; Adris, A. M. A Fluidized Bed Steam Reformer for Methane. *Proceedings of the VI International Fluidization Conference*, Banff, Canada, 1989; AIChE: New York, 1989; Vol. 319.

(3) Adris, A. M.; Elnashaie, S. S. E. H.; Hughes, R. A Fluidized Bed Membrane Reactor for the Steam Reforming of Methane. *Can. J. Chem. Eng.* **1991**, *69*, 1061.

(4) Adris, A. M. A fluidized bed membrane reactor for steam reforming: experimental verification and model validation. Ph.D. Dissertation, University of British Columbia, Vancouver, British Columbia, Canada, 1994.

(5) Adris, A. M.; Lim, C. J.; Grace, J. R. The Fluidized Bed Membrane Reactor for Steam Methane Reforming: Model Verification and Parametric Study. *Chem. Eng. Sci.* **1997**, *52*, 1609.

(6) Adris, A. M.; Grace, J. R.; Lim, C. J.; Elnashaie, S. S. E. H. Fluidized Bed Reaction System for Steam/Hydrocarbon Reforming to Produce Hydrogen. U.S. Patent 5,326,550, 1994.

(7) Roy, S.; Pruden, B. B.; Adris, A. M.; Lim, C. J.; Grace, J. R. Fluidized-bed Steam Methane Reforming With Oxygen Input. *Chem. Eng. Sci.* **1999**, *54*, 2095.

(8) Kikuchi, E. Membrane Reactor Application to Hydrogen Production. *Catal. Today* **2000**, *56*, 91.

(9) Kikuchi, E.; Nemoto, Y.; Kajiwara, M.; Uemiya, S.; Kojima, T. Steam Reforming of Methane in Membrane Reactors: Comparison of Electroless Plating and CVD Membranes and Catalyst Packing Modes. *Catal. Today* **2000**, *56*, 75.

(10) Lin, Y. S. Microporous and Dense Inorganic membranes: Current Status and Perspective. *Sep. Purif. Technol.* **2001**, *25*, 39.

(11) Nam, S.; Lee, K. Hydrogen Separation by Pd Alloy Composite Membranes: Introduction of Diffusion Barrier. *J. Membr. Sci.* **2001**, *192*, 177.

(12) Nam, S.; Lee, S.; Lee, K. Preparation of a Palladium Alloy Composite Membrane Supported in a Porous Stainless Steel by Vacuum Electrodeposition. *J. Membr. Sci.* **1999**, *153*, 163.

(13) Prabhu, A. K.; Liu, L. G.; Lovell, S. T.; Oyama, S. T. Modeling of the Methane Reforming Reaction in Hydrogen Selective Membrane Reactors. *J. Membr. Sci.* **2000**, *177*, 83.

(14) Uemiya, S. State-of-the-art of Supported Metal Membranes for Gas Separation. *Sep. Purif. Methods* **1999**, *28* (1), 51.

(15) Balasubramanian, B.; Lopez Ortiz, A.; Kaytakoglu, S.; Harrison, D. P. Hydrogen from Methane in a Single Step Process. *Chem. Eng. Sci.* **1999**, *54*, 3543.

(16) Silaban, A.; Harrison, D. P. High-Temperature capture of Carbon Dioxide: Characteristics of the Reversible Reaction Between CaO(s) and CO_2(g). *Chem Eng. Commun.* **1995**, *137*, 177.

(17) Ashcroft, A. T.; Cheetham, A. K.; Foord, J. S.; Green, M. L. H.; Grey, C. P.; Murrell, A. J.; Vernon, P. D. F. Selective Oxidation of Methane to Synthesis Gas Using Transition Metal Catalysts. *Nature* **1990**, *344*, 319.

(18) Bharadwaj, S. S.; Schmidt, L. D. Synthesis Gas Formation by Catalytic Oxidation of Methane in Fluidized Bed Reactors. *J. Catal.* **1994**, *146*, 11.

(19) De Groote, A. M.; Froment, G. F. Simulation of the Catalytic Partial Oxidation of Methane to Synthesis Gas. *Appl. Catal. A* **1996**, *138*, 245.

(20) Dissanayake, D.; Rosynek, M. P.; Kharas, K. C. C.; Lungsford, J. H. Partial Oxidation of Methane to Carbon Monoxide and Hydrogen over a Ni/Al_2O_3 Catalyst. *J. Catal.* **1991**, *132*, 117.

(21) Jin, R.; Chen, Y.; Li, W.; Cui, W.; Ji, Y.; Yu, C.; Jiang, Y. Mechanism for Catalytic Partial Oxidation of Methane to Syngas over a Ni/Al_2O_3 Catalyst. *Appl. Catal. A* **2000**, *201*, 71.

(22) Mleczko, L.; Wurzel, T. Experimental Studies of Catalytic partial Oxidation of Methane to Synthesis Gas in a Bubbling-bed Reactor. *Chem. Eng. J.* **1997**, *66*, 193.

(23) Jin, W.; Gu, X.; Li, S.; Huang, P.; Xu, N.; Shi, J. Experimental and Simulation Study on a Catalyst Packed Tubular Dense Membrane Reactor for Partial Oxidation of Methane to Syngas. *Chem. Eng. Sci.* **2000**, *55*, 2617.

(24) Tsai, C.; Dixon, A. G.; Moser, W. R.; Ma, Y. H. Dense Perovskite Membrane Reactors for Partial Oxidation of Methane to Syngas. *AIChE J.* **1997**, *43* (11A), 2741.

(25) Trimm, D. L. The Formation and Removal of Coke from Nickel Catalyst. *Catal. Rev.—Sci. Eng.* **1977**, *16* (2), 155.

(26) Bartholomew, C. H. Carbon Deposition in Steam Reforming and Methanation. *Catal. Rev.—Sci. Eng.* **1982**, *24* (1), 67.

(27) Chen, Z.; Yan, Y.; Elnashaie, S. S. E. H. Modeling and Optimization of a Novel Membrane Reformer for Higher Hydrocarbons. *AIChE J.* **2003**, *49* (5), 1250.

(28) Chen, Z.; Prasad, P.; Elnashaie, S. S. E. H. The Coupling of Catalytic Steam Reforming and Oxidative Reforming of Methane To Produce Pure Hydrogen in a Novel Circulating Fast Fluidization Bed Membrane Reformer. 223rd ACS National Meeting, Orlando, FL, April 7−11, 2002.

(29) Prasad, P.; Elnashaie, S. S. E. H. Novel Circulating Fluidized-Bed Membrane Reformer for the Efficient production of Ultraclean Fuels from Hydrocarbons. *Ind. Eng. Chem. Res.* **2002**, *41* (25), 6518.

(30) Prasad, P.; Elnashaie, S. S. E. H. Novel Membrane Circulating Fluidized Bed Reformer for the Efficient Production of Hydrogen from Natural Gas. 14th World Hydrogen Energy Conference, Montreal, Canada, June 9−13, 2002.

(31) Grace, J. R.; Li, X.; Lim, C. J. Equilibrium Modeling of Catalytic Steam Reforming of Methane in membrane Reactor with Oxygen Addition. *Catal. Today* **2001**, *64* (3−4), 141.

(32) Xu, J.; Froment, G. F. Methane Steam Reforming, Methanation and Water Gas Shift—I. Intrinsic Kinetics. *AIChE J.* **1989**, *35*, 88.

(33) Elnashaie, S. S. E. H.; Adris, A. M.; Al-Ubaid, A. S.; Soliman, M. A. On the Non-Monotonic Behavior of Methane Steam Reforming Kinetics. *Chem. Eng. Sci.* **1990**, *45* (2), 491.

(34) Ritchie, J. T.; Richardson, J. T.; Luss, D. Ceramic Membrane Reactor for Synthesis Gas Production. *AIChE J.* **2001**, *47* (9), 2092.

(35) Kim, J.; Lin, Y. S. Synthesis and Oxygen-Permeation Properties of Thin YSZ/Pd Composite Membranes. *AIChE J.* **2000**, *46* (8), 1521.

(36) Kunii, D.; Levenspiel, O. Circulating Fluidized-Bed Reactors. *Chem. Eng. Sci.* **1997**, *52*, 2471.

Received for review January 24, 2003
Revised manuscript received June 12, 2003
Accepted June 13, 2003

IE030071H